International Journal of Applied Electromagnetics and Mechanics 44 (2014) 301–315
DOI 10.3233/JAE-141793
IOS Press

Influence of a multiaxial stress on the reversible and irreversible magnetic behaviour of a 3%Si-Fe alloy

Mahmoud Rekik[a,b,*], Olivier Hubert[a] and Laurent Daniel[b,c]
[a]*LMT-Cachan, ENS Cachan, PRES Universud Paris, Cachan, France*
[b]*LGEP, SUPELEC, CNRS, UPMC, Univ Paris-Sud, Gif sur Yvette, France*
[c]*School of Materials, University of Manchester, Manchester, UK*

Abstract. The research presented in this paper is motivated by the design of electrical devices submitted to mechanical stress. It aims at studying the magnetic behaviour of ferromagnetic materials submitted to biaxial stress. It deals with the evolution of the magnetic susceptibility, coercive field and magnetic losses with respect to stress, magnetic field level and frequency. These quantities are of primary importance in the design of rotors for high speed rotating machines.
The work is focused on the magnetic behaviour of a standard grade of Iron-Silicon alloy under the form of thin sheet. Non conventional experiments are performed on cross-shaped samples in order to apply biaxial stress representative of the loadings experienced by rotors of rotating machines. These experiments are performed on a multiaxial testing machine, ASTREE. The magnetic loading is applied using a single U-yoke. The measurement of magnetic induction, magnetic field and strain is conducted by the means of needle-B sensor, H-coil sensors and Digital Image Correlation (DIC) respectively. Both anhysteretic and dissipative responses to magneto-mechanical loadings are considered. The results allow to identify the more critical stress configurations for this material.

Keywords: High speed rotating machines, biaxial stress, iron-silicon alloy, anhysteretic behaviour, dissipative behaviour, coercive field, power losses

1. Introduction

Electrical parts of an aircraft represent approximately 35% of the mass of equipment in the electrical power chain. In addition, the electrical power to be released on new generation of aeronautics equipment is multiplied by 4 compared to conventional aircraft. This induces an exponential increase in the number, mass and size of electrical equipment. To achieve the objectives of weight reduction it is mandatory to find appropriate solutions to optimize electrical systems. One solution is to increase the power density of generators. This requires higher rotation speed, leading to higher levels of centrifugal forces and stress in the rotor [1]. This speed contribution to stress comes in addition to other stress sources that can be inherited from forming and assembly processes (cutting, stacking, welding, ...).

The objective of this paper is to give experimental evidence of the influence of stress on the properties of electrical steels under biaxial stress for several frequency regimes. The magnetic material of

*Corresponding author: Mahmoud Rekik, LMT-Cachan, ENS Cachan, CNRS (UMR8535), UPMC, PRES Universud Paris, 61 Avenue du Président Wilson, 94235 Cachan, France. Tel.: +33 1 47 40 77 62; E-mail: rekik@lmt.ens-cachan.fr.

1383-5416/14/$27.50

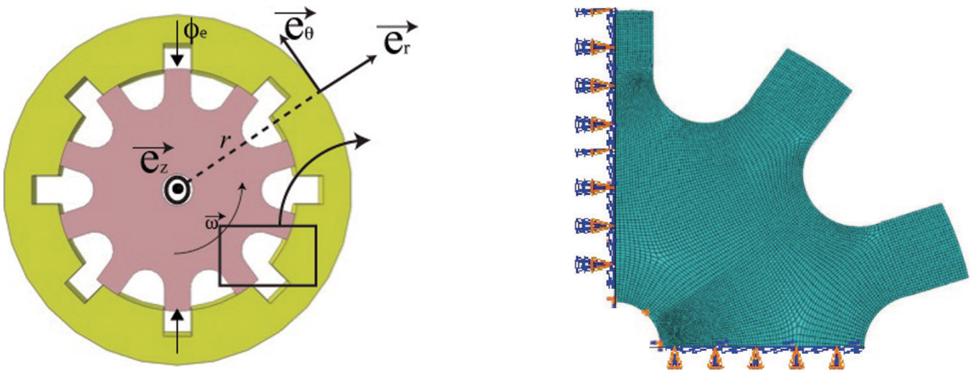

(a) Variable frequency generator (b) Boundary conditions and mesh

Fig. 1. Example of rotor/stator geometry of a high speed-rotating machine.

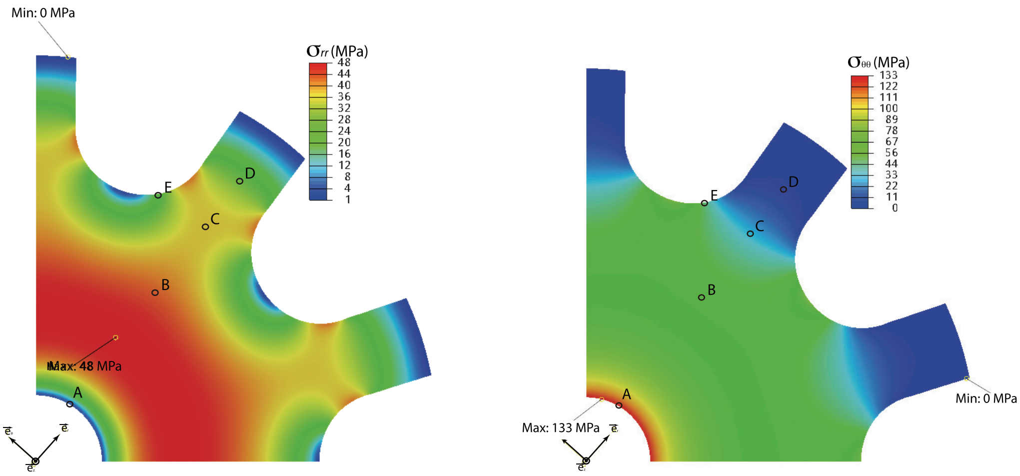

Fig. 2. Calculated radial (σ_{rr}) and tangential ($\sigma_{\theta\theta}$) inertial stress distribution in the rotor.

interest in this study is a commercial non-oriented 3%Si-Fe from Arcelormittal delivered in 0.5 mm thick sheets. It is a standard material for rotating machines. A precise understanding of the complex magneto-mechanical coupling effects in this material is necessary in order to perform accurate magneto-mechanical structural analysis on electromagnetic devices. In Section 2 the stress associated to centrifugal forces in a rotor is evaluated on a standard geometry for high speed rotating machine. In Section 3 the experimental setup for multiaxial magneto-mechanical characterisation is described and the results are presented and discussed in Sections 4 and 5.

2. Multiaxial stress in rotating machines

Modern technologies of wound rotor synchronous alternators for aeronautical applications involve higher and higher rotating speed and torque. High rotation speed creates high level of centrifugal forces. The first step of our analysis consists in estimating the stress experienced by a rotor under such high speed configurations. The analysis is limited here to the stress associated to centrifugal forces, but other

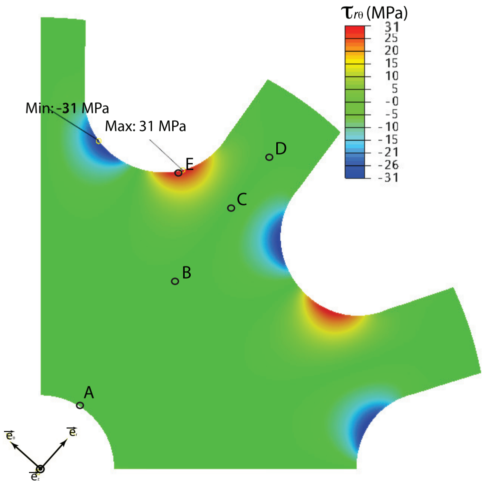

Fig. 3. Calculated shear ($\tau_{r\theta}$) inertial stress distribution in the rotor.

sources of stress could be superimposed (e.g. magnetic forces, torque..). A finite element modelling of a sheet metal rotor at angular velocity $\boldsymbol{\omega} = \omega.\mathbf{e}_z$ has been performed using the finite element code ABAQUS©. Figure 1(a) shows the geometry of the chosen rotor.

Volume forces are radial (Eq. (1)), ρ is the mass density and r the radial position.

$$\mathbf{f}_v = \rho r \omega^2 \, \mathbf{e}_r \tag{1}$$

A quarter of the rotor is modelled. Figure 1(b) shows the mesh and the boundary conditions corresponding to the symmetry of the problem. Considering the small thickness of the sheet ($e = 0.5$ mm) simulations are realized under plane stress assumptions. Local stress is calculated at each node of the mesh. The resulting stress tensor is under the form of Eq. (2) in cylindrical coordinates.

$$\boldsymbol{\sigma} = \begin{pmatrix} \sigma_{rr} & \tau_{r\theta} \\ \tau_{r\theta} & \sigma_{\theta\theta} \end{pmatrix} \tag{2}$$

The calculated components of the stress tensor in the rotor are plotted in Figs 2 and 3 for the angular velocity $\omega = 4190$ rad.s^{-1} (40,000 rpm). The material properties have been taken isotropic in the sheet plane. The Young modulus is $E = 191$ GPa, the Poisson ratio $\nu = 0.27$ and the mass density $\rho = 7870$ kg.m^{-3} (usual values for iron-silicon alloys [2,3]). The external radius of the rotor is $r_{\max} = 38.0$ mm and the internal radius is $r_{\min} = 26.5$ mm.

The stress tensor has been extracted and reported in Eq. (3) for a few points of interest A, B, C, D and E placed on the figures. The stress intensity is proportional to the angular velocity (values are reported for 40,000 rpm).

$$\boldsymbol{\sigma}_A = \begin{pmatrix} 0 & 0 \\ 0 & 133 \end{pmatrix} \quad \boldsymbol{\sigma}_B = \begin{pmatrix} 46 & 0 \\ 0 & 64 \end{pmatrix} \quad \boldsymbol{\sigma}_C = \begin{pmatrix} 37 & -10 \\ -10 & 20 \end{pmatrix}$$
$$\boldsymbol{\sigma}_D = \begin{pmatrix} 20 & 0 \\ 0 & 2 \end{pmatrix} \quad \boldsymbol{\sigma}_E = \begin{pmatrix} 25 & 30 \\ 30 & 46 \end{pmatrix} \quad \text{(MPa)} \tag{3}$$

σ_{rr} and $\sigma_{\theta\theta}$ are positive on the entire structure. $\tau_{r\theta}$ is almost zero in most of the rotor except near the lower edges of the rotor teeth where stress concentration occurs (e.g. points C and E). Bi-tension

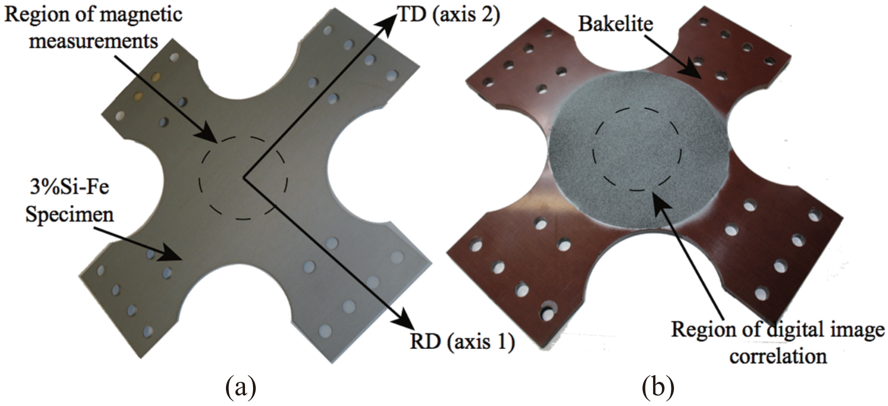

Fig. 4. Experimental two-layer specimen: (a) specimen geometry; (b) core material: Bakelite and speckle used for DIC.

($\sigma_{rr} > 0, \sigma_{\theta\theta} > 0, \tau_{r\theta} = 0$) is the configuration the most encountered within the material (e.g. points B and D). The orthoradial stress $\sigma_{\theta\theta}$ is often the dominant component of the stress tensor and can reach the double of σ_{rr} in some areas (e.g. point E). In the teeth of the rotor, $\sigma_{\theta\theta}$ vanishes so that σ_{rr} becomes the dominant component of the stress tensor (e.g. point D). The region near the axis of the rotor experiences high intensity tensile stress in the orthoradial direction (e.g. point A), and the external edges of the teeth are almost unstressed. The magnitude of stress is significant (of the order of a few tens of MPa) but remains far from the yield stress of the material (approximately 360 MPa). This finite element analysis illustrates the multiaxiality and the non-uniformity of stress within the rotor of a rotating machine.

3. Experimental procedure

The characterisation of magneto-mechanical behaviour is usually performed under uniaxial conditions [2,3]. The stress consists then of pure tension or compression applied along an axis parallel to the magnetic field. Such experiments cannot cover the complex interactions between stress and magnetic field under more general magneto-mechanical loadings. Biaxial magneto-mechanical loading conditions can provide a deeper insight into magneto-elastic couplings but very few are reported in the literature [4–12]. The basic idea of biaxial tests is to perform a measurement of magnetic behaviour on a specimen loaded in tension-compression along two perpendicular directions. For that purpose, a cross-shaped specimen has been designed (Fig. 4(a)). Compression tests can be carried out if the specimen is designed to prevent buckling. This can be achieved thanks to a central core stuck to the specimen (Fig. 4(b)). Bakelite can be chosen for the core material. It is non-magnetic and non-conductive so that it does not disturb the magnetic measurement. A local frame (1,2) is attached to the sheet with direction 1 corresponding to the rolling direction (RD) and direction 2 corresponding to the transverse direction (TD). The local stress tensor (σ_1, σ_2) in the centre of the specimen can be calculated from the forces applied along the two loading axes (F_1, F_2) according to an interacting matrix $[K]$ with non-diagonal terms ($\boldsymbol{\sigma} = [K].\mathbf{F}$). The terms of the matrix have been computed thanks to a finite element mechanical modelling of the specimen. The magnetic measurement area is a 30 mm diameter circle where both stress and magnetic field are fairly uniform (heterogeneity less then 15% [10]) (homogeneity of magnetic field has been verified for the same geometry in previous studies [12]).

Magnetic field and magnetic induction are measured thanks to a calibrated H-coil and a needle-B sensor respectively. Strain field is obtained thanks to Digital Image Correlation (DIC) on the Bakelite

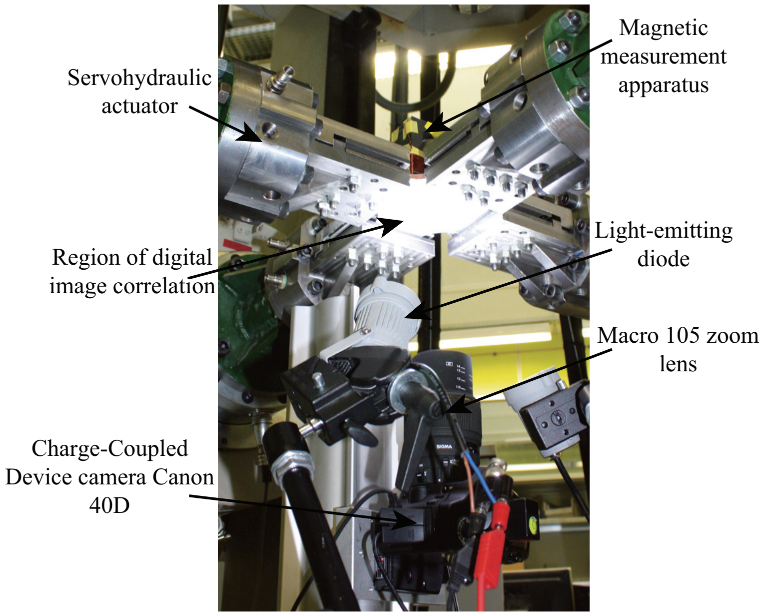

Fig. 5. Experimental setup for biaxial testing.

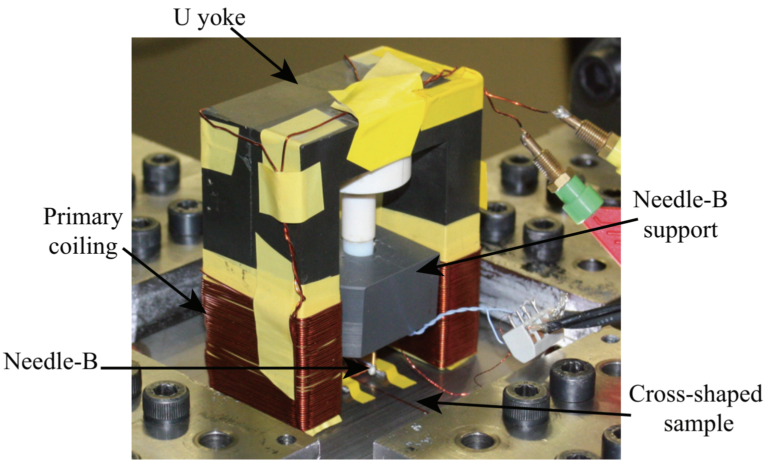

Fig. 6. Magnetic measurements: U yoke and sensors.

side of the specimen. Figure 5 is a picture of the experimental setup including the equipment used for DIC and Fig. 6 is a closer view on the specimen and the magnetic measurement apparatus put between the jacks of the hydraulic machine ASTREE.

The magnetic measurement procedure includes anhysteretic curves and hysteresis loops. Anhysteretic curves are constructed point after point by applying to the material a large amplitude alternating magnetic field superimposed on a dc magnetic field. The amplitude of the alternating field is slowly reduced to zero until only the dc field remains. This latter points defines the anhysteretic response corresponding to the applied dc field (Fig. 7). The material is demagnetised after each measurement of anhysteretic point to eliminate any influence of loading history in the measurement.

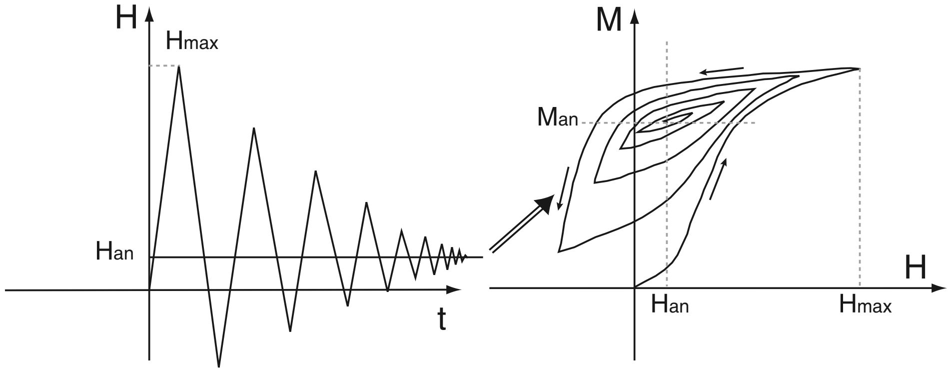

Fig. 7. Principle of measurement for one point of the anhysteretic curve.

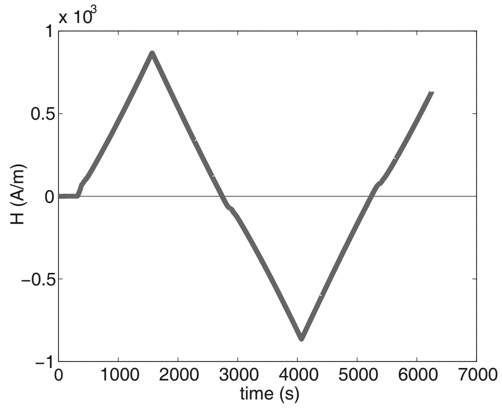

(a) Magnetic field H

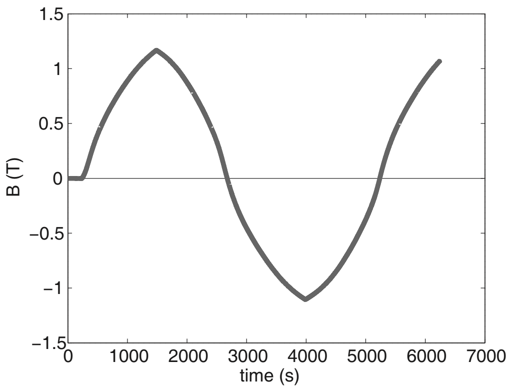

(b) Magnetic induction B

Fig. 8. Magnetic measurement output as a function of time.

The measurement of hysteresis loops has been carried out at frequency of $\{f\} = \{1, 5, 10, 50, 100, 200, 400, 800\}$ Hz. A triangular form of the current $i(t)$ has been used. The corresponding evolution of the measured magnetic field $H(t)$ is plotted in Fig. 8(a) and the magnetic induction $B(t)$ in Fig. 8(b). The magnetic field is slightly distorted and remains fairly triangular while the magnetic induction is strongly distorted due to the non linearity of the magnetic behaviour.

The results can then be extracted in the form of magnetic induction curves $B(H)$ or magnetization curves $M(H)$ (using $B = \mu_0(H + M)$). The remnant induction B_r, the coercive field H_c and the power losses P can be calculated from the hysteresis loops (Fig. 9). For a given value of the magnetic field H and associated magnetization M the secant susceptibility can also be defined: $\chi = M/H$.

For technical reasons related to the current command and non simultaneity f.e.m. measurement and integration, maximal induction can be subjected to a decrease at high frequencies (> 400 Hz). We define a correction factor r^i ($0.9 < r^i < 1$) which represents the ratio between the maximum induction $B^i_{\max}$ at given frequency ($i \in \{f\}$) and the maximum induction $B^1_{\max}$ at $f = 1$ Hz (Eq. (4)).

$$r^i = \frac{B^i_{\max}}{B^1_{\max}} \tag{4}$$

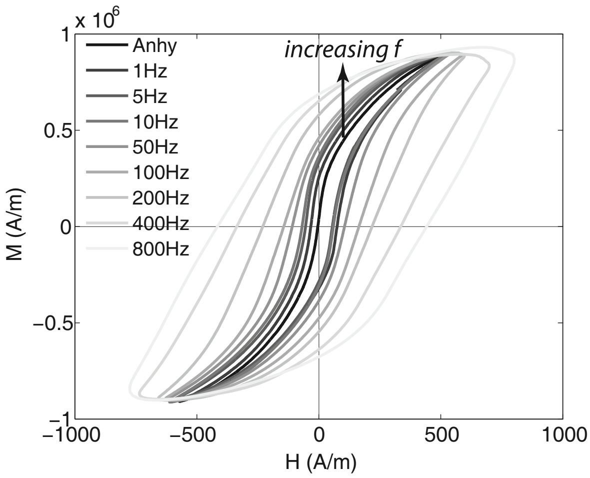

Fig. 9. Examples of hysteresis loops obtained at different frequencies for $(\sigma_1, \sigma_2) = (50, -50)$ MPa ($B_{\max} \simeq 1.1\ T$).

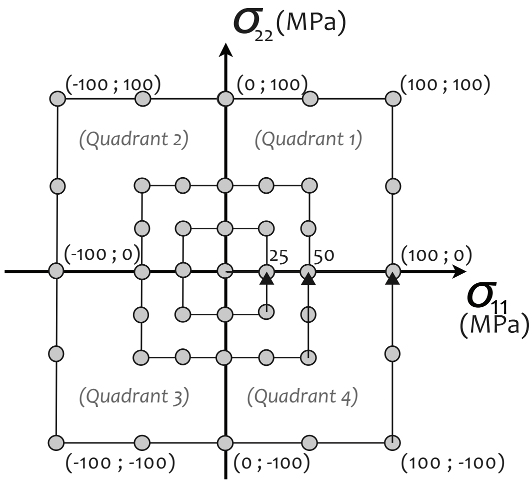

Fig. 10. Experimental points in the (σ_1, σ_2) plane and definition of 4 quadrants.

This correction allows the comparison of hysteretic parameters (H_c, B_r, P) at a given value of $B_{\max}$. A linear correction is applied so that (Eq. (5)):

$$\begin{aligned}(H_c^i)_{corrected} &= \frac{H_c^i}{r^i}\\ (B_r^i)_{corrected} &= \frac{B_r^i}{r^i}\\ (P^i)_{corrected} &= \frac{P^i}{r^i}\end{aligned} \tag{5}$$

The measurement procedure is applied for several biaxial mechanical loadings (σ_1, σ_2). The magnetic field is applied in the direction parallel to axis 1. 41 biaxial loading configurations have been tested, for stress level varying from -100 MPa to $+100$ MPa. These stress states are plotted in the (σ_1, σ_2) plane in Fig. 10.

4. Results

4.1. Anhysteretic magnetization curves

Magnetization curves under uniaxial stress are given in Fig. 11. Figure 11 shows the case of a parallel uniaxial stress for which the uniaxial stress is applied in the direction of the magnetic field. The stress configuration is then given by (σ_1,0). The compression progressively deteriorates the magnetic behaviour – the magnetic susceptibility decreases – while tension enhances the magnetic behaviour (for the stress levels reported here). In the case of a perpendicular uniaxial stress (Fig. 11(b)) for which the uniaxial stress is applied in the direction orthogonal to the magnetic field, the stress configuration is (0, σ_2). The effect of stress is significantly reduced in that configuration. The magnetic behaviour is slightly deteriorated during the first stages of magnetization and then slightly enhanced above 1000 A/m. The effect of tension is stronger than the effect of compression for a given stress intensity.

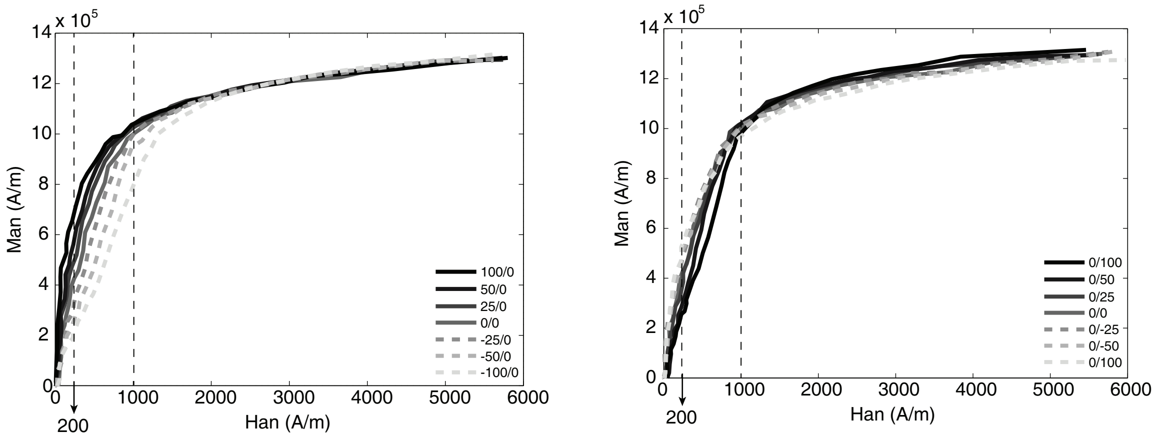

(a) Parallel uniaxial stress ($\sigma_2 = 0$) (b) Perpendicular uniaxial stress ($\sigma_1 = 0$)

Fig. 11. Anhysteretic magnetization curves under uniaxial stress.

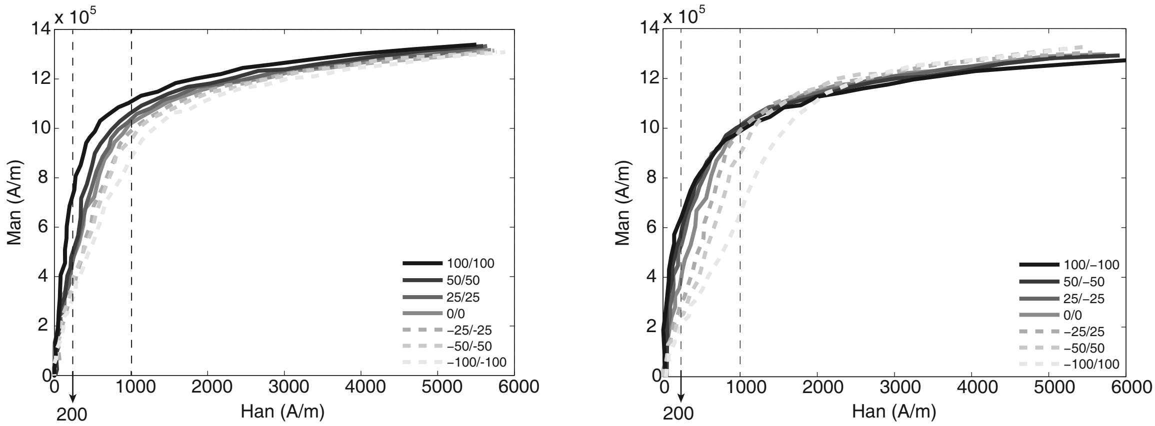

(a) Equibiaxial stress ($\sigma_1 = \sigma_2$) (b) Pure shear stress ($\sigma_1 = -\sigma_2$)

Fig. 12. Anhysteretic magnetization curves under biaxial stress.

Magnetization curves under biaxial stress are given in Fig. 12(a). Under equibiaxial stress configuration (Fig. 12), characterised by the condition $\sigma_1 = \sigma_2$, negative stress components deteriorate the magnetic behaviour while positive stress components slightly enhance it. This effect is similar but lower in magnitude compared with parallel uniaxial stress configuration. Pure shear stress can also be applied (Fig. 12(b) – $\sigma_1 = -\sigma_2$). The effect of pure shear is hardly sensitive when the component of stress (σ_1) parallel to the applied magnetic field is positive. But when σ_1 is negative, the deterioration of magnetic behaviour is very significant.

4.2. Secant susceptibility

The influence of a biaxial stress on the anhysteretic behaviour is discussed in terms of secant susceptibility $\chi = (M/H)$. Figures 13(a) and (b) plot the relative variation of secant susceptibility defined by

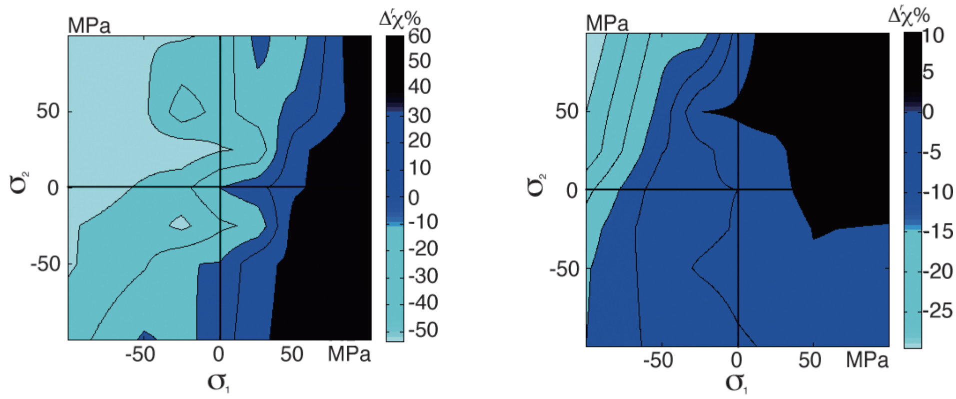

(a) H=200 A/m, $\chi^0_{200} = 2020$ (b) H=1000 A/m, $\chi^0_{1000} = 980$

Fig. 13. Relative variation $\Delta^r\chi$ of the secant magnetic susceptibility in the stress plane for a magnetic loading along RD.

Eq. (6) in the (σ_1, σ_2) plane. Two levels of magnetic field (shown in Figs 11 and 12) have been considered: $H = 200$ A/m (Fig. 13(a)) and $H = 1000$ A/m (Fig. 13(b)). The magnetic field is applied parallel to the rolling direction (RD).

$$\Delta^r\chi = 100 \times \frac{\chi(\sigma_1, \sigma_2) - \chi(0,0)}{\chi(0,0)} = 100 \times \frac{\Delta\chi}{\chi^0} \tag{6}$$

As already noticed in the previous section, a uniaxial tension along the magnetic field direction improves the susceptibility and a compression in the same direction deteriorates the magnetic behaviour. When a uniaxial stress is applied in the direction perpendicular to the magnetic field, the effect is opposite and attenuated. The tension-compression asymmetry is very perceptible. Bi-tension increases the susceptibility (${\Delta\chi^r}_{200}^{100,100} = 60\%$), while bi-compression decreases it (${\Delta\chi^r}_{200}^{-100,-100} = -50\%$). The lowest values of χ are obtained in the second quadrant of the graph, corresponding to shear configurations. A compression along the magnetic field direction always tends to deteriorate the magnetic behaviour, whatever the value of σ_2. It can also be noticed that a bi-tension tends to slightly increase the magnetic susceptibility χ. The effects of stress are less sensitive at high levels of magnetic field since the material is closer to saturation.

4.3. Coercive field

The relative variations $\Delta^r H_c$ of the coercive field H_c under biaxial loading are given in Fig. 14. These variations are calculated with respect to the unstressed configuration according to:

$$\Delta^r H_c = 100 \times \frac{H_c(\sigma_1, \sigma_2) - H_c(0,0)}{H_c(0,0)} = 100 \times \frac{\Delta H_c}{H_c^0} \tag{7}$$

It can be noticed that the variation $\Delta^r H_c$ is symmetric with respect to the line $\sigma_1 = -\sigma_2$. This variation is attenuated with increasing frequency. A strong similarity can be observed between the plots at low frequency ($f < 200$ Hz). Under such frequencies the region of minimum coercive field is the fourth quadrant ($\sigma_1 > 0, \sigma_2 < 0$) corresponding to shear stress with positive stress component along the magnetic field direction. Along the line of pure shear stress ($\sigma_1 = -\sigma_2$) in the second quadrant ($\sigma_1 < 0$,

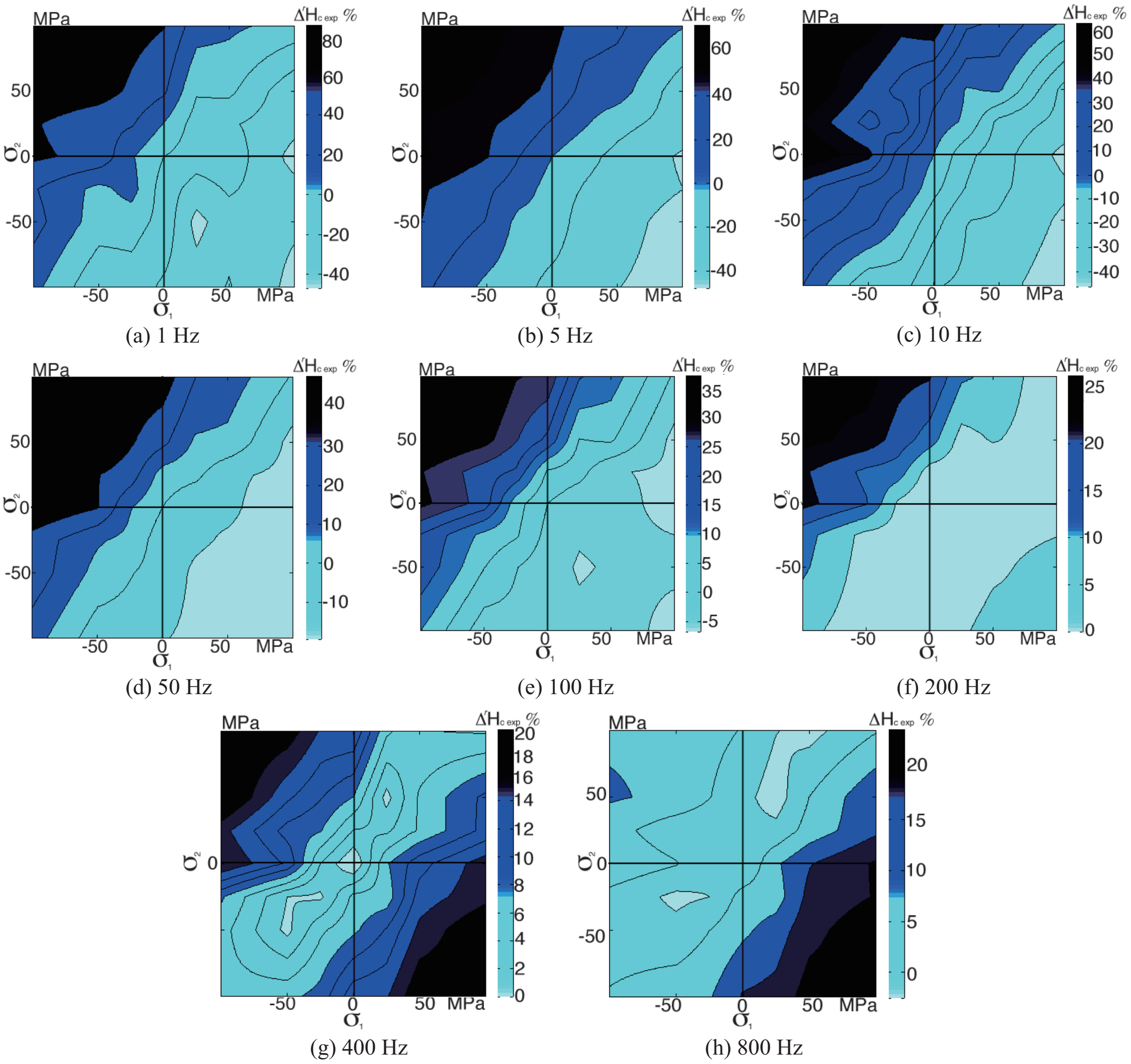

Fig. 14. Variations $\Delta^r H_c$ of coercive field under biaxial stress at different frequencies.

$\sigma_2 > 0$), there is a strong increase of H_c when the stress intensity is getting higher. This leads to the conclusion that shear stress has a very strong effect on the coercive field when the component of stress along the magnetic field direction is negative, but negligible otherwise. At frequencies of 400 Hz and higher, effect of stress on the coercive field is changing. The variations observed are lower. The area of minimum effect of stress becomes the equibiaxial region close to the line $\sigma_1 = \sigma_2$. The maximum coercive field values are still observed for shear stress but now in the fourth quadrant, for positive σ_1. At 400 Hz, a symmetry with respect to the line $\sigma_1 = \sigma_2$ is observed in addition to the symmetry with respect to the line $\sigma_1 = -\sigma_2$.

4.4. Power losses

The relative variations $\Delta^r P$ of the power losses P under biaxial loading are given in Fig. 15. These

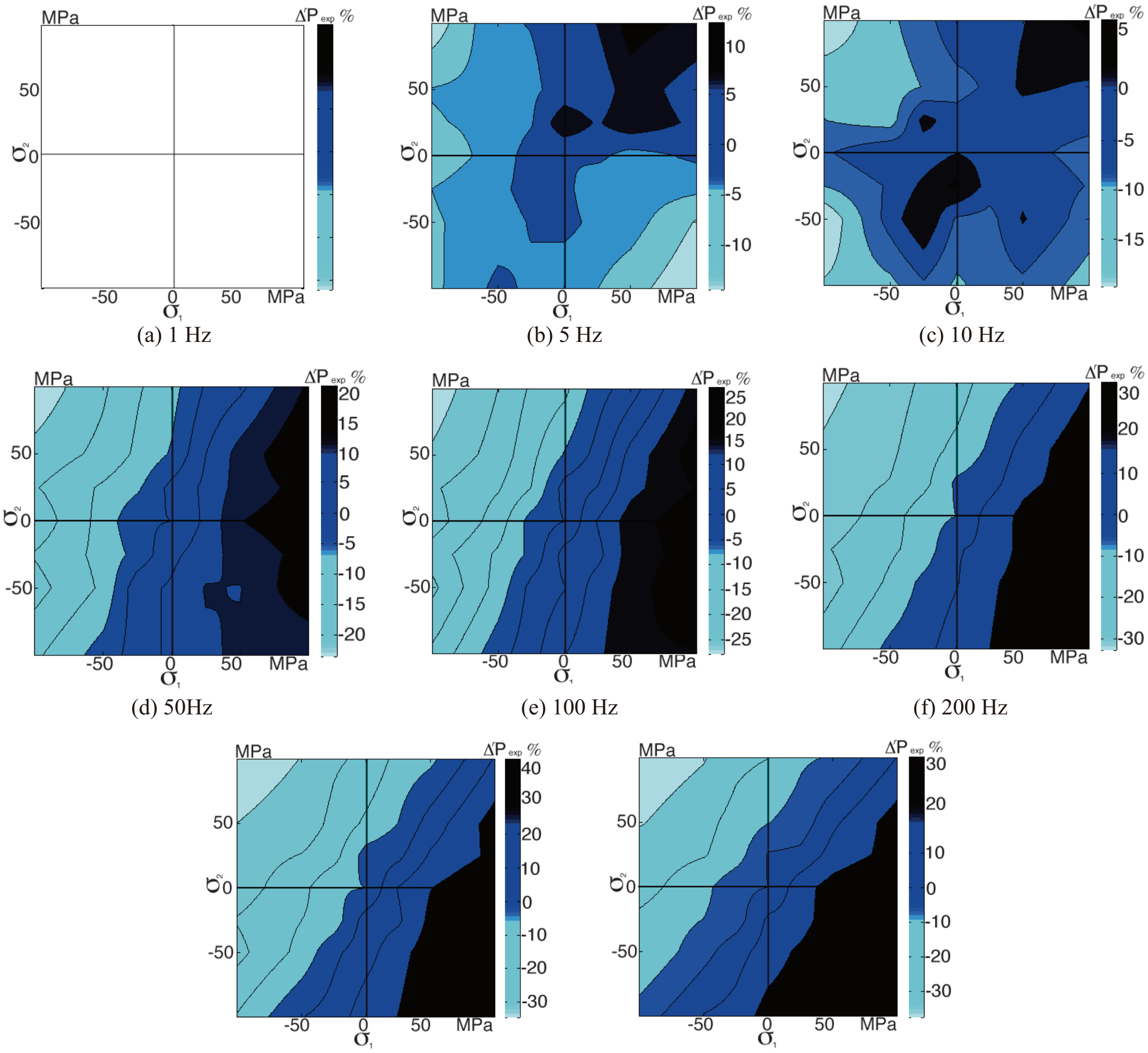

(a) 1 Hz (b) 5 Hz (c) 10 Hz

(d) 50Hz (e) 100 Hz (f) 200 Hz

(g) 400 Hz (h) 800 Hz

Fig. 15. Variations $\Delta^r P$ of power losses under biaxial stress at different frequencies.

variations are calculated with respect to the unstressed configuration according to:

$$\Delta^r P = 100 \times \frac{P(\sigma_1, \sigma_2) - P(0,0)}{P(0,0)} = 100 \times \frac{\Delta P}{P^0} \tag{8}$$

The power losses at 1 Hz are not presented in Fig. 15 because the calculated value are very low ($P_{\text{max}} \simeq 0.025$ W/kg) and associated to large uncertainties. For frequencies below 10 Hz the effect of stress on power losses is slight. A bi-tension state tends to increase the magnetic power losses (by approximately 5% for $\sigma_1 = \sigma_2 = 100$ MPa). The highest power losses are obtained along the equibiaxial line $\sigma_1 = \sigma_2$. For frequencies of 50 Hz and higher, the trends observed in the figures are very different.

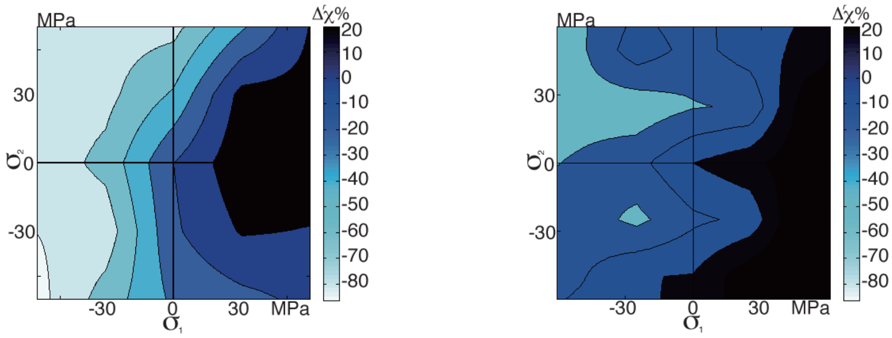

(a) Iron-Cobalt alloy [12], $H = 250$ A/m, $\chi^0_{250} = 5000$

(b) Iron-Silicon alloy [this study], $H = 200$ A/m, $\chi^0_{200} = 2020$

Fig. 16. Relative variation $\Delta^r\chi$ of the secant magnetic susceptibility under biaxial mechanical loading.

The highest power losses are now obtained for high positive σ_1. At 50 Hz this effect is almost independant of σ_2 but when the frequency increases the role of σ_2 becomes more significant. A negative σ_2 tends to increase the power losses. At high frequencies the highest power losses are obtained under shear stress with positive σ_1 (fourth quadrant). The iso-values of power losses are almost vertical lines at 50 Hz but the slope – positive – is decreasing apparently towards a slope of 1 as the frequency gets higher. The lowest power losses are obtained for shear stress with negative σ_1 (second quadrant).

5. Discussion

5.1. *Secant susceptibility*

The results obtained in this work can be compared with the results obtained by Hubert [12] with a similar test rig on 0.5 mm thick sheets of an Iron-Cobalt alloy (49%Co-49%Fe-2%V). The anhysteretic secant susceptibility was measured at 250 A/m under biaxial stress loadings with maximum magnitude of 60 MPa for each component. The results are plotted in Fig. 16(a) and the results of the present study are recalled in Fig. 16(b).

The tension-compression asymmetry is easily perceptible on both graphs. The predominant role of the stress component along the magnetic field is also a common feature of the two figures. But while the degradation under compressive parallel stress is dramatic for Iron-Cobalt it is moderate for the Iron-Silicon alloy. The increase of magnetic susceptibility under tensile stress is moderate for Iron-Cobalt whereas it is spectacular for the Iron-Silicon alloy. The iso-values of susceptibility are mainly directed in a vertical direction but this comparison highlights the complexity of the effects of stress on magnetic behaviour and notably their great dependency to the considered material.

5.2. *Coercive field*

The results obtained in this work can be compared with the results obtained by Pearson et al. [12] at medium frequency (50 Hz) on 1 mm thick sheets of pure Iron. The variations of coercive field were measured under biaxial stress loadings with maximum magnitude of 30 MPa for each component. The results are plotted in Fig. 17(a) and the results of the present study are recalled in Fig. 17(b). The main trends seem similar on both figures.

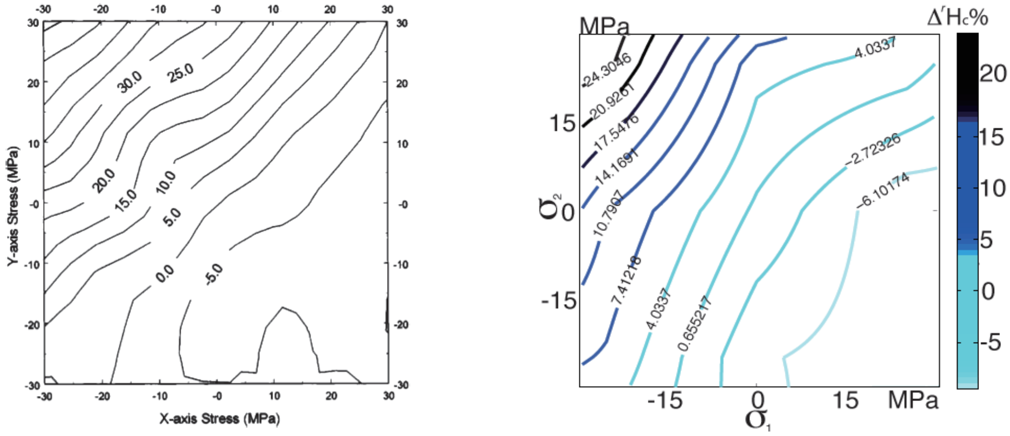

(a) Pure Iron [9] (b) Iron-Silicon alloy [this study]

Fig. 17. Variations $\Delta^r H_c$ of coercive field under biaxial stress at $f = 50$ Hz.

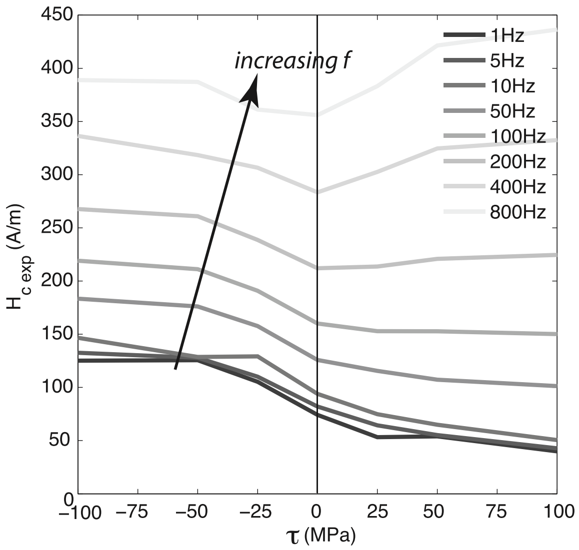

Fig. 18. Coercive field under pure shear stress ($\sigma_1 = -\sigma_2$) as a function of shear stress intensity $\tau = \frac{1}{2}(\sigma_1 - \sigma_2)$ at different frequencies.

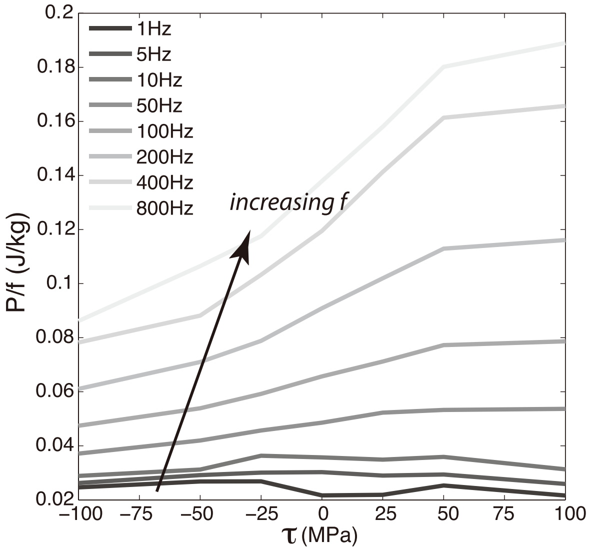

Fig. 19. Power losses per cycle under pure shear stress ($\sigma_1 = -\sigma_2$) as a function of shear stress intensity $\tau = \frac{1}{2}(\sigma_1 - \sigma_2)$ at different frequencies.

It is also interesting to look at the influence of frequency. To highlight the interaction of stress with frequency, the coercive field H_c under pure shear loading as a function of the shear stress intensity τ ($\tau = \frac{1}{2}(\sigma_1 - \sigma_2)$) is plotted in Fig. 18 at different frequencies. Indeed it was observed on the hysteresis loops that shear stress configurations have a strong effect on the coercive field, and that the pure shear line ($\sigma_1 = -\sigma_2$) was an axis of symmetry in Fig. 14.

It is evident from Fig. 18 that the effect of stress and frequency are coupled. At low frequency an increasing shear stress tends to decrease the coercive field while it tends to increase the coercive field at high frequency. Again this observation points out the complexity of the effects of stress on magnetic behaviour.

5.3. Power losses

The same analysis on frequency effects can be made on power losses. Figure 19 shows the measured power losses per cycle P/f under pure shear loading as a function of the shear stress intensity τ ($\tau = \frac{1}{2}(\sigma_1 - \sigma_2)$) at different frequencies.

Eddy currents induced in the specimen cause significant losses. Above 100 Hz, flux is mainly concentrated at the surface due to the skin effect, resulting in an increase of eddy current losses. On the other hand the change in permeability due to stress also affects the skin depth.

Another important issue confirming the interpretation is that the slope of iso-values of P (Fig. 15) in the eigen stress frame is increasing with frequency, aligning with the slope of iso-values of permeability.

At this step, a parallel can be made between core losses, susceptibility and coercive field evolutions with stress. It seems clear that losses evolution (especially at high frequency) is correlated with susceptibility evolution (increase of micro and macro eddy currents with higher permeability, skin depth). Conversely, low frequency coercive field reduces with applied stress exhibiting the so-called refinement phenomenon of domains as usually observed in Grain-Oriented silicon steels [2,3]. With increasing frequency, losses contribution to coercivity progressively increases leading to a progressive change of coercivity sensitivity to stress.

6. Conclusion

An experimental setup dedicated to observe the influence of biaxial stress and frequency on the magnetic behaviour of thin soft magnetic materials was described.

The obtained results for iron-silicon are consistent with the results published in previous work concerning susceptibility and coercive field. Experimental results of power losses evolution with biaxial stress and frequency provide a new contribution to the knowledge in the field.

All results confirm the pre-dominant role of the stress component along the magnetic field axis. Nevertheless the change of magnetic quantities with stress does not seem to follow the same rule depending on the magnetic quantity considered. On the other hand coercive field and power losses exhibit both a coupling with frequency strongly dependent to the stress. Accurate design of high speed rotating machines requires consequently numerical models taking into account these effects. Such numerical models do not exist today.

Multiscale phenomenological approaches are an interesting solutions [13,14]. But they refer to anhysteretic behaviour which is a strong limitation. This should be overcome.

Acknowledgment

The authors wish to thank Arcelormittal for providing the material and 3MT FUI-OSEO Project for the financial support.

References

[1] L. Bernard, X. Mininger, L. Daniel, G. Krebs, F. Bouillault and M. Gabsi, Effect of stress on switched reluctance motors: A magneto-elastic finite-element approach based on multiscale constitutive laws, *IEEE Trans Magn* **47**(9) (2011), 2171–2178.

[2] R.M. Bozorth, Ferromagnetism, Van Nostrand Company, New York, 1951, pp. 595–712.
[3] B.D. Cullity and C.D. Graham, Introduction to magnetic materials, Wiley, New Jersey, 2011, pp. 241–273.
[4] C.S. Schneider and J.M. Richardson, Biaxial magnetoelasticity in steels, *J Appl Phys* **53** (1982), 8136–8138.
[5] K. Kashiwaya, Magnetoelastic effect of 3.25% Si-Fe single crystal under low magnetic field, *J Appl Phys* **31** (1992), 237–250.
[6] M.J. Sablik, L.A. Riley, G.L. Burkhardt, H. Kwun, P.Y. Cannell, K.T. Watts and R.A. Langman, Micromagnetic model for the influence of biaxial stress on hysteretic magnetic properties, *J Appl Phys* **75** (1994), 5673–5675.
[7] M.J. Sablik, Smith, Q. Marina, C.J. Waldhart, D.A. McKee and B. Augustyniak, The effects of biaxial stress on Barkhausen noise signals when the magnetic field is noncoaxial with the stress axes, *J Appl Phys* **84** (1998), 6239–6249.
[8] M.J. Sablik, B. Augustyniak and M. Chmielewski, Modeling biaxial stress effects on magnetic hysteresis in steel with the field and stress axes noncoaxial, *J Appl Phys* **85** (1999), 4391–4393.
[9] J. Pearson, P.T. Squire, M.G. Maylin and J.G. Gore, Biaxial stress effects on the magnetic properties of pure iron, *IEEE Trans Magn* **36** (2000), 3251–3253.
[10] V. Maurel, F. Ossart, Y. Marco and R. Billardon, Setup to test biaxial stress effect on magnetomechanic coupling, *J Appl Phys* **93** (2003), 7115–7117.
[11] O. Hubert, M. Chaabane, J. Jumel, V. Maurel, F. Alves, A.D. Bensalah, M. Besbes, K. Azoum, L. Daniel and F. Bouillault, A new experimental set-up for the characterization of magneto-mechanical behaviour of materials submitted to biaxial stresses, Application to FeCo alloys, *EL Rev/Prz Elektr* **81** (2005), 19–23.
[12] O. Hubert, Influence of biaxial stresses on the magnetic behavior of an iron-cobalt sheet experiments and modelling, *EL Rev/Prz Elektr* **83**(4) (2007), 70–77.
[13] L. Daniel, O. Hubert, N. Buiron and R. Billardon, Reversible magneto-elastic behavior: A multiscale approach, *J Mech Phys Solids* **56** (2008), 1018–1042.
[14] O. Hubert and L. Daniel, Energetical and multiscale approaches for the definition of an equivalent stress for magneto-elastic couplings, *J Magn Magn Mater* **323**(20) (2011), 1766–1781.